Non-destructive testing on creep degraded 12% Cr-Mo-W-V ferritic test samples using Barkhausen noise

Bhaawan Gupta, Benjamin Ducharne, Tetsuya Uchimoto, Gaël Sebald, Takamichi Miyazaki, Toshiyuki Takagi

▶ **To cite this version:**

Bhaawan Gupta, Benjamin Ducharne, Tetsuya Uchimoto, Gaël Sebald, Takamichi Miyazaki, et al.. Non-destructive testing on creep degraded 12% Cr-Mo-W-V ferritic test samples using Barkhausen noise. Journal of Magnetism and Magnetic Materials, 2020, 498, pp.166102. 10.1016/j.jmmm.2019.166102 . hal-02458830

HAL Id: hal-02458830
https://hal.science/hal-02458830

Submitted on 11 Apr 2022

HAL is a multi-disciplinary open access archive for the deposit and dissemination of scientific research documents, whether they are published or not. The documents may come from teaching and research institutions in France or abroad, or from public or private research centers.

L'archive ouverte pluridisciplinaire **HAL**, est destinée au dépôt et à la diffusion de documents scientifiques de niveau recherche, publiés ou non, émanant des établissements d'enseignement et de recherche français ou étrangers, des laboratoires publics ou privés.

Non-destructive Testing on Creep Degraded 12% Cr-Mo-W-V Ferritic Test Samples using Barkhausen Noise

Bhaawan Gupta[1, 2, 3], Benjamin Ducharne[2], Tetsuya Uchimoto[1, 3], Gael Sebald[1], Takamichi Miyazaki[4], Toshiyuki Takagi[1,3]*

[1]ELyTMaX UMI 3757, CNRS – Université de Lyon – Tohoku University, International Joint Unit, Tohoku University, Sendai, Japan
[2]Univ Lyon, INSA-Lyon, LGEF, EA682, F-69621, Villeurbanne, France
[3]Institute of Fluid Science, Tohoku University, Sendai, Japan
[4]Instrumental Analysis Group, Graduate School of Engineering, Tohoku University, Sendai, Japan

Abstract

Micro-magnetic non-destructive testing helps in evaluating the mechanical and structural integrity of ferromagnetic components (mostly steel) via local magnetic characterization. As a means of revealing the magnetic domain wall movements, the Barkhausen noise measurement method is a micro-magnetic non-destructive testing method of considerable potential and interest. The Magnetic Barkhausen Noise Energy (MBN_{energy}) method can be used to reconstruct local hysteresis cycles from Barkhausen noise measurements. These cycles constitute good indicators for understanding the magnetization process and the influence of microstructural and mechanical properties. In this article, the MBN_{energy} method is employed for evaluating the microstructural changes induced by creep/ageing of high chromium steel subjected to different creep test conditions as stress and temperature. The corresponding magnetic parameters are investigated in relation to precipitations and dislocations. After the experimental analysis, simulations are performed based on the Jiles-Atherton theory for the quasi-static magnetic behavior. This simulation approach yields physically meaningful model parameters that can be analyzed and linked to the sample microstructural characteristics, thereby enabling physical interpretation.

Keywords

Magnetic Barkhausen Noise, Electromagnetic Non-destructive testing, Micro-magnetic modeling, high chromium steel, creep degradation, Jiles-Atherton model

1. Introduction

Micro-magnetic non-destructive testing (NDT) can be used to evaluate the mechanical properties (such as the hardness and ageing level) of materials. The Barkhausen noise is very sensitive to mechanical changes and residual stresses [1]–[4]. These mechanical changes may lead to microstructural changes and magnetic-behavior modifications. The microstructural changes modify the domain wall movements and, hence, Barkhausen noise measurements represent an interesting means of investigating load-induced phenomena such as creep [1][2][5][6]. Studying creep in materials helps to reveal the level of rupture for a material subjected to a given set of conditions [7]. Several factors (such as dislocations, recovery of the crystallization stage, and variations in the carbide precipitates) contribute to the creep in materials. Eventually, these factors all lead to the formation of cracks and material failure after a certain threshold. Creep has been a very important matter of concern for the power plant industries [8][9].

Recently, the application of micro-magnetic non-destructive techniques, such as measuring the magnetic Barkhausen noise (MBN), has increased considerably in industrial fields [3]. This is due mainly to the improvement of signal processing techniques that have enabled and simplified the online production monitoring [4]. However, industrial implementation is limited because the reproducibility of the raw signal results mainly from the acquisition process completed by high-order

*Corresponding author.
E-mail address: gael.sebald@insa-lyon.fr (Gael Sebald)

filters and huge-gain amplifier stages. The Magnetic Barkhausen Noise Energy (MBN_{energy}) method can be used to reconstruct local hysteresis cycles from Barkhausen noise measurements. These hysteresis cycles constitute good indicators for understanding the magnetization process and the influence of microstructural and mechanical properties. The integration step filters the raw signal and provides a stable image of the Barkhausen noise and is therefore a quite efficient tool. In this work, the MBN_{energy} method is employed for the evaluation of microstructural changes due to creep in 12 % Cr-Mo-W-V creep steel samples. These samples were previously investigated via the Magnetic Incremental Permeability (MIP) technique described in the previous work of the authors. The motivation is to determine the microstructural characteristics from the magnetic parameters derived from the MBN signal. To avoid repeatability issues due to the sensor, lift off, and sensibility (such as the quest of the most sensitive indicator), as per [10] [11], MBN_{energy} hysteresis cycles will be plotted and evaluated. MBN_{energy} hysteresis cycles are obtained by plotting the time integration of the squared Barkhausen noise multiplied by the excitation field time derivation sign as a function of H, see equation 1; Bark(t) is the raw MBN signal:

$$MBN_{energy}(t) = \left(\int_0^t Bark(t')^2 . sign\left(\frac{dH}{dt} \right) dt' \right) \quad (1)$$

As in the case of the classical hysteresis cycles considering the average induction field B versus the tangential magnetic excitation H, MBN_{energy} hysteresis cycles area are related to an energy.
A raw Barkhausen noise signal can be considered an image of the domain wall speed. By integrating the square of the signal (see Equation (1)) the area of the resulting hysteresis cycle is obtained as an image of the kinetic energy. This energy is consumed by the domain walls during the magnetization process. After the experimental analysis, the magnetic signals are modeled using the theory of Jiles-Atherton for quasi-static conditions. The model parameters derived in the case of MBN are analyzed and linked to the sample microstructural characteristics, thereby enabling physical interpretation.

2. Experimental procedure

Fig. 1 shows a schematic of the experimental set-up. The tested samples are magnetically excited using a sinusoidal magnetic excitation field driven with the help of a soft U-shaped magnetic lamination stack.
The samples are all of the same size, for further details see [7]. The yoke is fabricated from silicon steel sheets, the leg size is 10 mm x 20 mm, and the inner-distance between legs is 20 mm. The excitation frequency is set to 0.1 Hz after optimization tests, as explained in the previous study [7]. The excitation magnetic field is feedback controlled to ensure a 10 kA/m maximum amplitude. Furthermore, the sensor used to pick up the Barkhausen Noise signal consists of two pancake pick-up coils and a Hall Effect sensor located inside. The Hall sensor measures the tangential surface excitation field H, on the surface of the tested sample. The output of the pick-up coils is transmitted to an electronic analog circuit. These coils operate independently, a commune potential is set, and the differential voltage is amplified. This circuit uses a differential amplifier (P-61, NF Corporation) to provide a first amplification (by a factor of 1000) of the differential Barkhausen signal. Once amplified, this signal is fed to a band pass filter (BPF) with a 1–60 kHz cut off frequency. The output of the BPF is amplified again by a factor of 50 prior to the oscilloscope acquisition. In parallel, the output of the Hall sensor is also amplified by a factor of 50 prior to acquisition by the oscilloscope. The raw MBN signal can be measured directly or processed, as suggested in [11], to obtain the $MBN_{energy}(H)$ curve.

*Corresponding author.
E-mail address: gael.sebald@insa-lyon.fr (Gael Sebald)

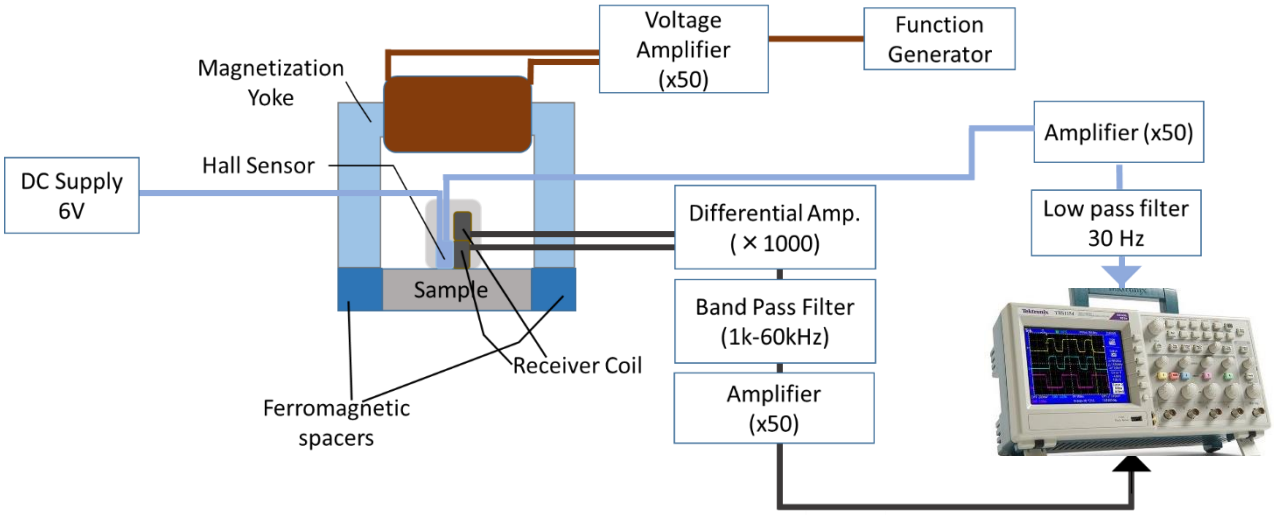

Figure 1. Magnetic Barkhausen Noise Measuring System (Schematic)

For this, in a second electronic circuit, the square of the Barkhausen noise is first calculated using an *AD633* analog multiplier, followed by a low noise operational amplifier *OPA2604* in an integration configuration ensuring the integration of the signal. A small reed relay *D31C2100* provides the reset function of the integrator as soon as the acquisition is completed. Fig. 2 shows all the signals acquired by the oscilloscope. Signal 1 (Blue), Signal 2 (Cyan), and Signal 3 (Red) are the output of the Hall sensor, raw amplified magnetic Barkhausen noise, and square of the MBN (Signal 2), respectively. Signal 4 (Green) is the integrated output of Signal 3. A post processing numerical treatment is performed for the drift correction, sign of the MBN_{energy} time derivation, cycle symmetry, and final plot.

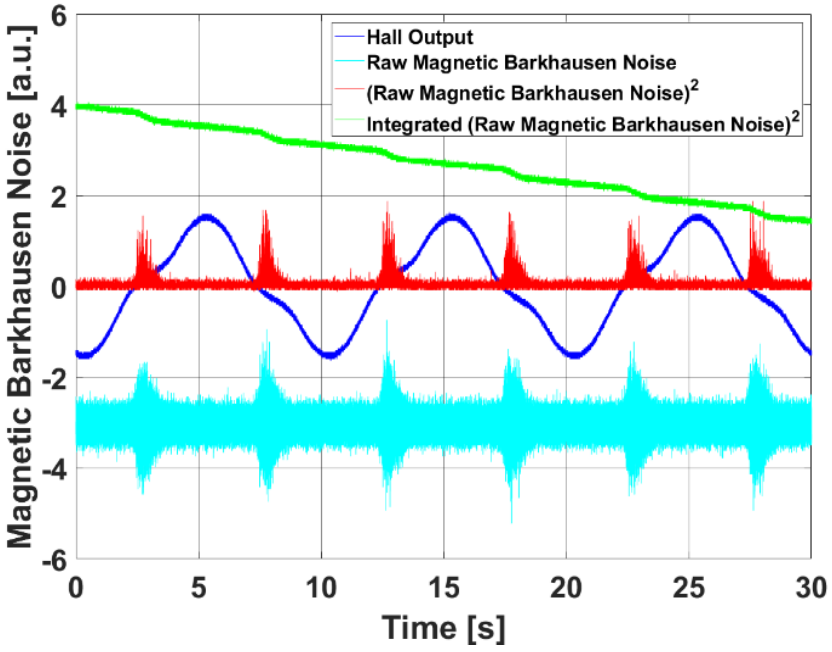

Figure 2. Data Acquisition for the Magnetic Barkhausen Noise Measurement system

*Corresponding author.
E-mail address: gael.sebald@insa-lyon.fr (Gael Sebald)

3. Materials of Interest and Microstructural Evaluation

3.1. Sample description

In this study, three different categories of samples are investigated. For each category, every investigated sample is characterized by a different rupture level. The material considered in the present study, i.e., a 12% Cr-Mo-W-V steel, is a representative martensitic stainless steel (the general composition of this alloy is given in [12]). Such alloys are used for high-temperature material applications including steam gas turbines and boilers. The percentages of the samples tested in our study may vary slightly, but we assume that changes in the magnetic behavior due to these weak variations will be extremely limited.

Table 1 provides a short description of the sample conditions. The Larson Miller Parameter is a statistical parameter that combines the effect of Temperature T and test time t in a mathematical expression [13], and is given as follows:

$$LMP = T(C + \log t) \tag{2}$$

Where, *C* is a material specific constant, often taken as ~20, *t* is the time in hours, and *T* is the temperature in Kelvin. The values of LMP for each sample are calculated and presented in Table 1, which is given as follows:

Table 1. List of Samples

Sample number	Stress [MPa]	Temp [°C]	Test time [h]	LMP*
0	-	-	-	-
1	343	550	281.8	18479
2	343	550	785.6	18846
3	343	550	2205.7	19215
4	201	600	255.6	19565
5	201	600	763.9	19980
6	201	600	1725.9	20289
7	98	650	256.3	20686
8	98	650	789.6	21137
9	98	650	1736.8	21453

Larson Miller Parameter

3.2. Microstructural analysis

The microstructure of each sample was analyzed via Scanning Electron Microscopy and Electron Backscatter Diffraction (EBSD), which yields the Kernel Average misorientation (KAM) data. The KAM is defined as the average misorientation angle of a given point with all its neighbors [14] [15]. Further details of the standard procedures are provided in [14] [15], with [15] describing previous work by the authors where the MIP technique is employed. In the present work, we try to relate these data with the Barkhausen Noise signal and then use a modeling technique for further quantification to derive parameters that describe the correlation between the signal and the microstructure. Fig. 3 shows the most relevant data results obtained from the microstructural analysis. Previous work [7] [15] on these samples by the current authors has provided a detailed analysis of the results.

*Corresponding author.
E-mail address: gael.sebald@insa-lyon.fr (Gael Sebald)

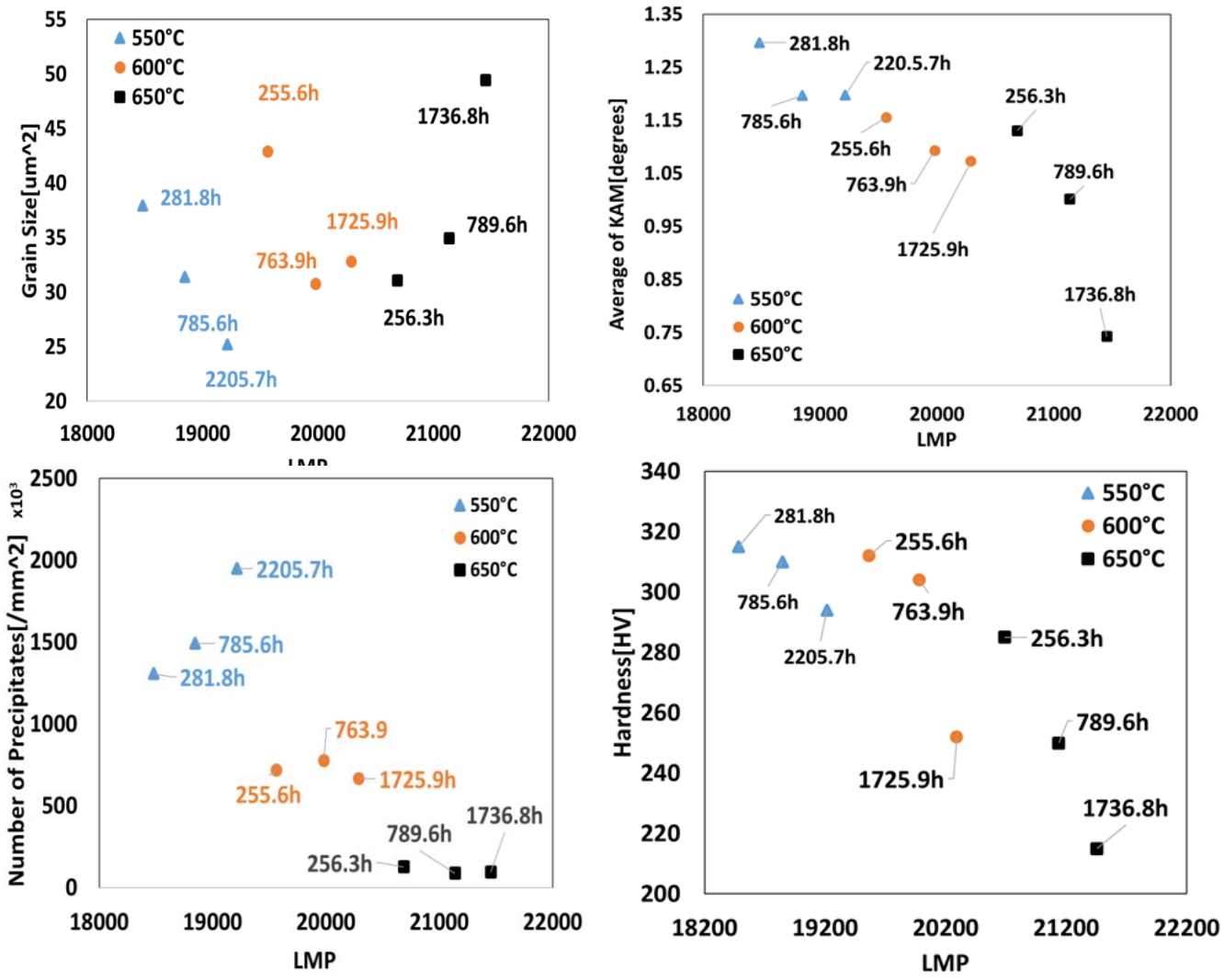

Figure 3: Microstructural Data Evaluation

4. Experimental Results

Hysteresis cycles constructed from magnetic Barkhausen noise raw signals are referred to as $MBN_{energy}(H)$ cycles. Fig. 4 shows the different steps of this reconstruction. During the first step (b), the square of the raw signal is calculated. The resulting signal is multiplied by sign(dH/dt), which is 1 with increasing H and -1 otherwise. A time integration is performed immediately after, as illustrated in Fig. 4(c), and the offset is removed. Afterward, a normalization step is performed to ensure equality between the absolute value of both the MBN_{energy} maximum and the minimum.

4.1. Experimental Data Analysis of 12%Cr-Mo-W-V Creep Test Samples

Fig. 5(a) shows the raw magnetic Barkhausen Noise signal for the three 550°C samples. Fig. 5(b) shows the comparison of these three different samples via the reconstructed MBNenergy Hysteresis cycles from the raw MBN signal, using the technique presented in Fig. 4. From the raw signal, clear differences are observed between the samples. The amplitude of the raw signal decreases with increasing creep. Clear differences among the saturation points of the three samples are observed and the coercivity of the ruptured sample is observed to be higher than that of Sample 1. This results from the number of precipitates, which is considerably higher than the number occurring in Sample 1, leading to magnetically hard samples as rupture is approached.

*Corresponding author.
E-mail address: gael.sebald@insa-lyon.fr (Gael Sebald)

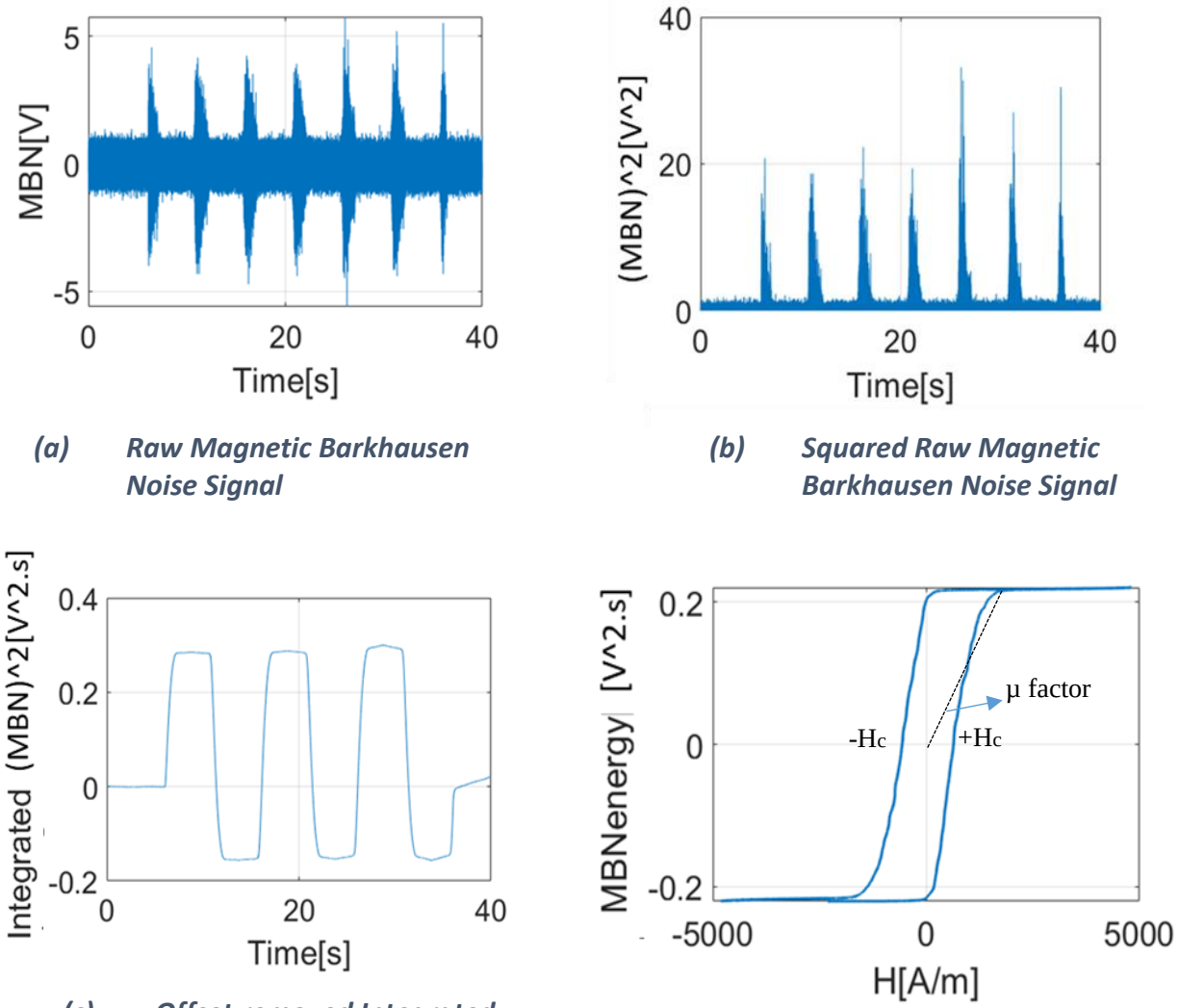

(a) ***Raw Magnetic Barkhausen Noise Signal***

(b) ***Squared Raw Magnetic Barkhausen Noise Signal***

(c) ***Offset removed Integrated MBN Signal***

(d) ***Offset removed Integrated MBN Signal vs. H***

Figure 4. Derivation of MBN_{energy} cycle from Raw Magnetic Barkhausen Noise

*Corresponding author.
E-mail address: gael.sebald@insa-lyon.fr (Gael Sebald)

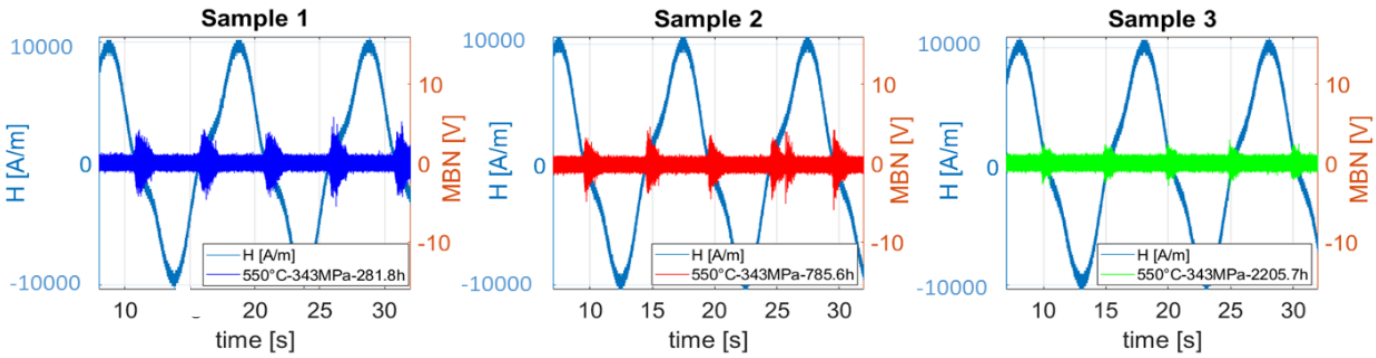

(a) Raw MBN signals for samples 1–3

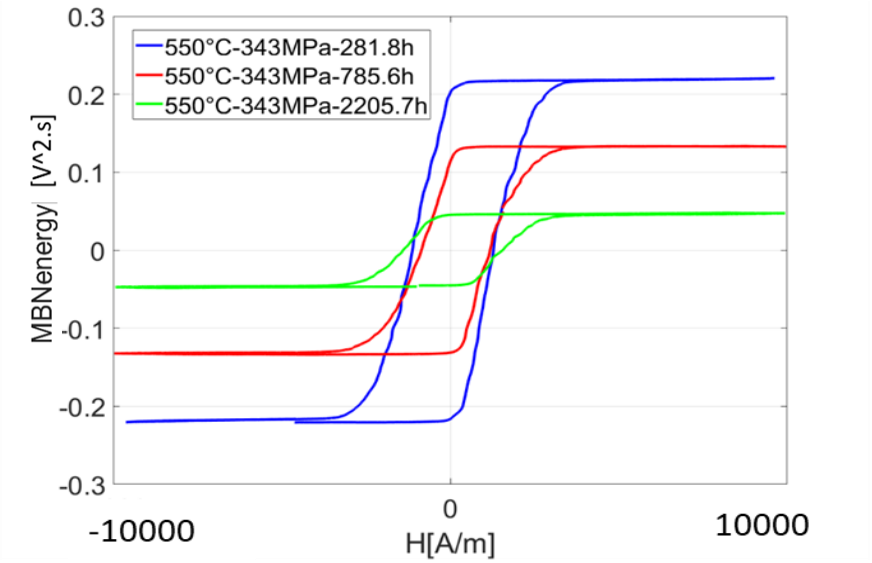

(b) Reconstructed MBN_{energy} cycles for samples 1–3

Figure 5. Raw MBN signal for Samples 1–3 and their respective reconstructed MBN_{energy} Hysteresis cycles (Bottom)

Fig. 6 shows the comparison of the samples from the 600°C category. As in the case of the MIP results in [7], the results differ slightly among the different samples. However, from the MBN_{energy} hysteresis cycles, the differences in the magnitude of MBN_{energy} are quite noticeable. The MBN activity in the raw signals decreases over time as the rupture level increases.

*Corresponding author.
E-mail address: gael.sebald@insa-lyon.fr (Gael Sebald)

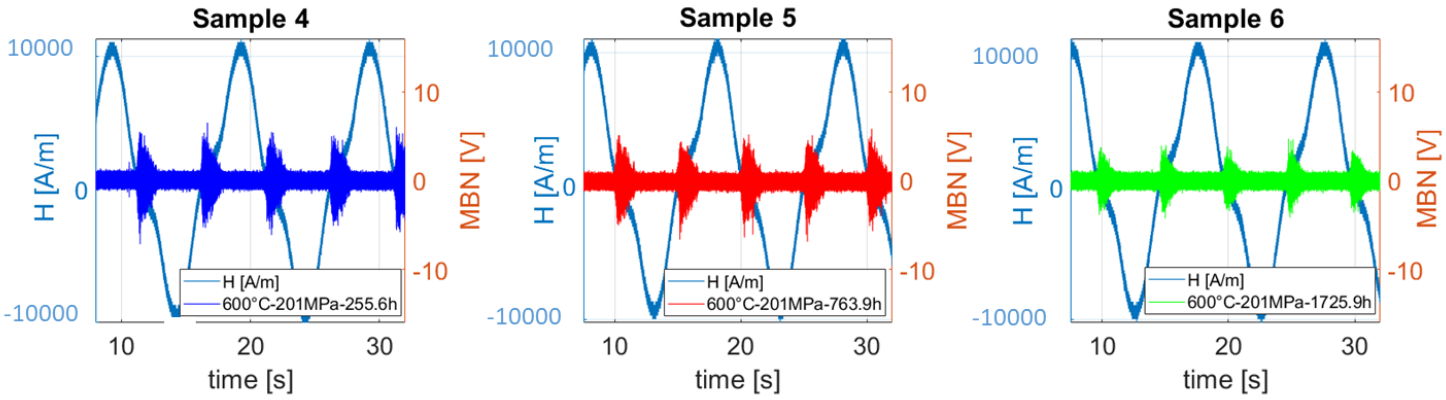

(a) Raw MBN signals for samples 4–6

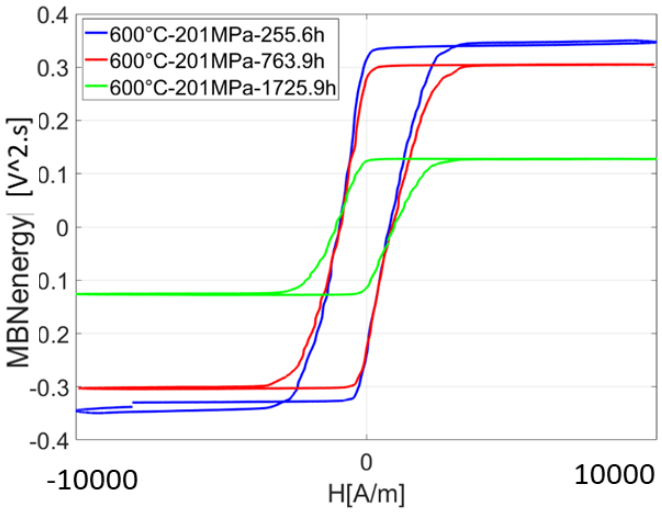

(b) Reconstructed MBN_{energy} cycles for samples 4–6

Figure 6. Raw MBN signal for Samples 4–6 and their respective reconstructed MBN_{energy} Hysteresis cycles (Bottom)

Fig. 7 shows the comparisons for the 650°C category of samples. In contrast to the 550°C samples, the amplitude of the MBN of these samples increases with increasing rupture level. Moreover, the Barkhausen noise activity decreases with increasing time and when rupture is close. In this case, again

*Corresponding author.
E-mail address: gael.sebald@insa-lyon.fr (Gael Sebald)

in contrast to the 550°C samples, the coercivity of the loops also decreases as the rupture nears.

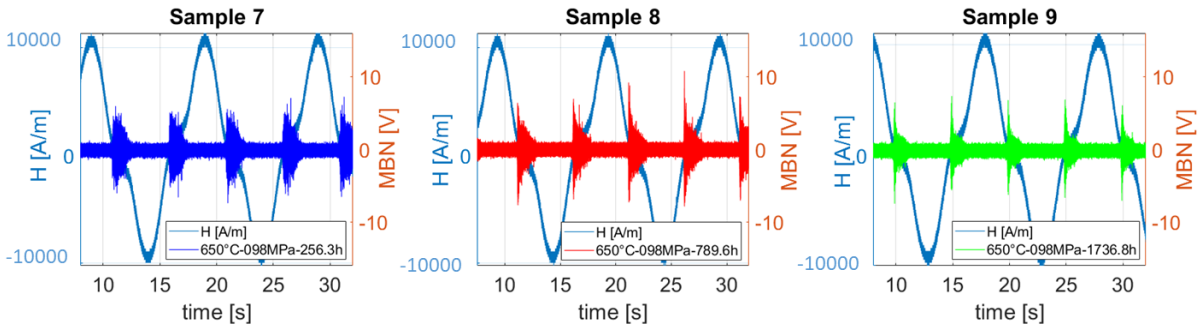

(a) Raw MBN signals for samples 7–9

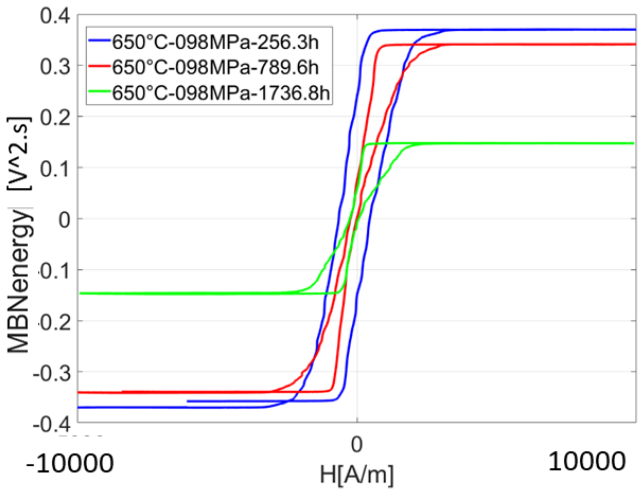

(b) Reconstructed MBN_{energy} cycles for samples 7–9

Figure 7. Raw MBN signal for Samples 7–9 and their respective reconstructed MBNenergy Hysteresis cycles (Bottom).

4.2. Comparison among the ruptured samples from the three different categories

Fig. 8 shows the comparisons of the raw magnetic Barkhausen noise signals of the three ruptured

*Corresponding author.
E-mail address: gael.sebald@insa-lyon.fr (Gael Sebald)

samples from three different categories as well as their respective reconstructed MBN_{energy} hysteresis cycles. As the figure shows, the peak to peak voltage amplitude of the raw Barkhausen noise increases with increasing heat-treatment temperature of the samples. From a physical point of view, this can be interpreted as a softening of the magnetic properties, increasing of the permeability, and decreasing of the absolute values associated with the coercive fields. That is, the higher-temperature-treated samples are magnetized and demagnetized faster than the other samples. These results are confirmed by the $MBN_{energy}(H)$ cycle figure (see Fig. 8(b)).

From the microstructural analysis, for the 650°C samples, the number of precipitates is lower than in the other samples, thereby favoring easy domain wall movements. This leads to an easier orientation of the domains in the direction of the applied magnetic field, resulting in higher and more rapid magnetizability than in other directions. Furthermore, for samples treated at similar temperatures (Fig. 5), the coercivity increases (in general) with increasing rupture of the 550°C samples, but decreases in the case of the 650°C samples (Fig. 7). This may have resulted from the effect of the precipitates. At 550°C, the number of precipitates is dominant and at 650°C the size of the precipitates is dominant. Fewer misorientations/dislocations (KAM data can be found in section 3) occur, on average, in the higher-temperature-treated samples (than in the lower-temperature-treated samples), thereby resulting in quicker magnetization and higher permeability. Based on Figs. 5–7, from the MBN_{energy} curves, parameters such as the coercivity factor, permeability factor (µfactor) corresponding to the slope of the curves, and MBN_{energy} amplitude are extracted and correlated with the microstructure of the materials. However, when considering the amplitude of the MBN_{energy} curve, the absolute values for the same material may vary with different experimental set-ups, because of the gain factor, but the relative relation between the samples will always remain constant.

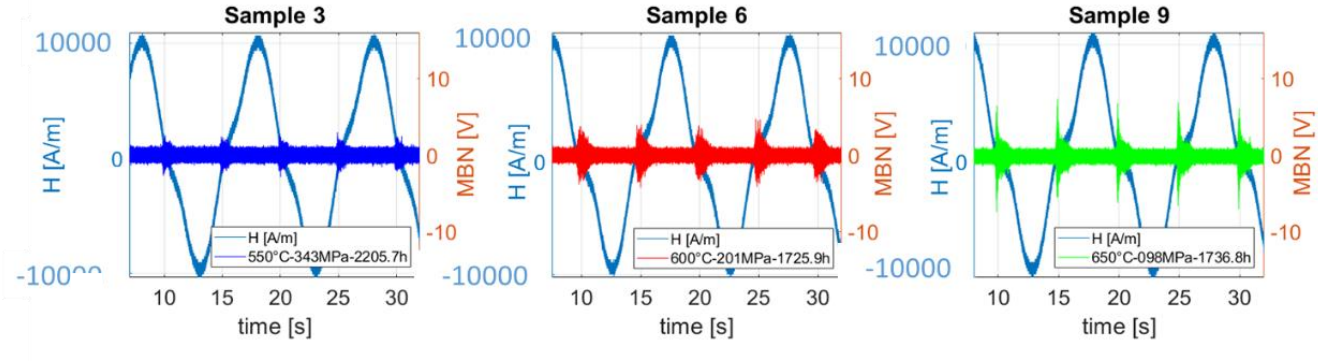

(a) Raw MBN signals for ruptured samples (Samples 3, 6, &9)

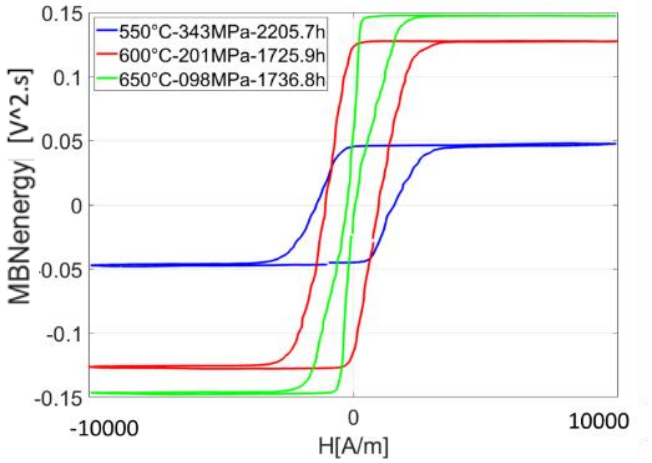

(b) Reconstructed MBN_{energy} cycles for ruptured samples (Samples 3, 6, &9)

Figure 8. Comparison of ruptured samples from three different temperature categories

*Corr
E-mail address: gael.sebald@insa-lyon.fr (Gael Sebald)

4.3. Magnetic parameters versus the microstructure

Figs. 9–10 show the correlation of magnetic parameters derived from MBN_{energy} curves with the microstructural characteristics of precipitates and dislocations (Fig. 3). The use of the Barkhausen noise measuring technique also demonstrates the effect of microstructural changes in the materials. The tendency of the parameters is similar to that of the MIP results [7]. The higher temperature samples behave in an opposite manner to the lower temperature samples. For example, the coercivity increases (in general) with increasing number of precipitates in the 550°C samples, leading to magnetic hardening of the materials. However, for the 600°C and 650°C samples, the coercivity decreases with decreasing number of precipitates, due to the soft magnetic behavior of the materials.
KAM is an important factor from a materials science point of view, but for an understanding of creep, satisfactory correlation between KAM and the magnetic parameters may be lacking. However, a larger variation is observed for the 650°C samples (as in the case of the MIP technique, B(H) technique, and the modeling parameters derived from those techniques [7] [15]) than for the other samples. The average density of dislocations decreases in the high-temperature samples, thereby resulting in higher permeability and magnetic reversibility. When the material is tested via the Barkhausen technique, the coercivity exhibits the strongest correlation with the microstructure, and this is also verified with the model, as demonstrated in Section 5.3.

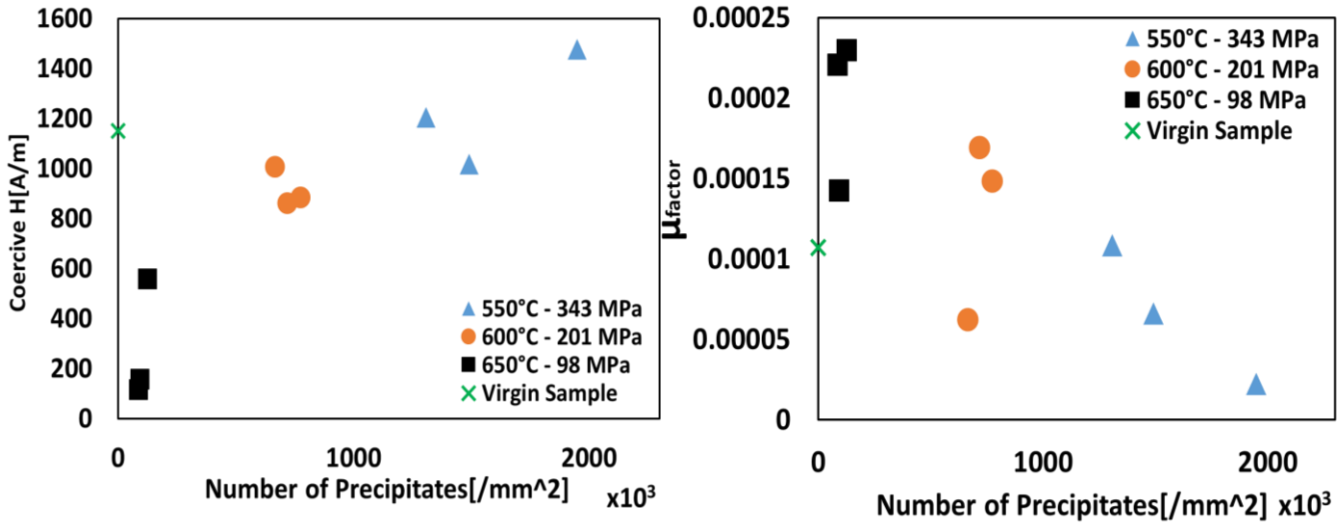

(a) Coercivity versus Precipitations

(b) Permeability factor versus Precipitations

Figure 9. Magnetic Parameters derived from MBN versus number of precipitates

*Corresponding author.
E-mail address: gael.sebald@insa-lyon.fr (Gael Sebald)

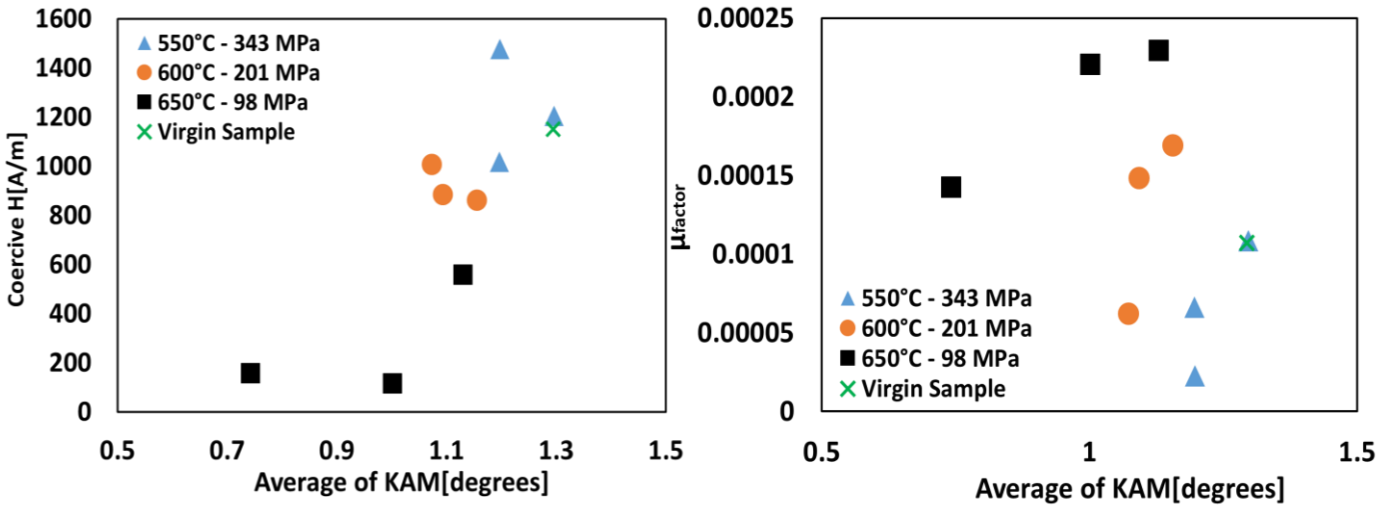

(a) Coercivity versus Average of KAM

(b) Permeability factor versus Average of KAM

Figure 10. Magnetic Parameters derived from MBN versus average of KAM

5. Jiles-Atherton hysteresis theory for the simulation of the MBN_{energy} hysteresis cycles

5.1. Introduction to the classic Jiles-Atherton (J-A) model

Below a frequency threshold, the cumulative periodic value of ferromagnetic losses becomes frequency independent (in the decreasing direction), and this represents the quasi-static state. This behavior is observable by plotting the spontaneous average magnetic induction *B* versus the tangential surface magnetic excitation field *H* under weak frequency (<< 1 Hz for a typical soft ferromagnetic). To obtain correct simulation results for this quasi-static hysteresis, the J-A model considers both contributions – the domain wall bending and the domain wall translations [16]–[18]. Additionally, the:

- model requires a fairly small memory storage, where the evolution history information is limited to a single time step before *B*;
- status can be completely described by five physically meaningful and interdependent parameters;
- J-A model is easily reversible (*H* or *B* can serve as input for the model) [19][20].

In the scalar J-A model for ferromagnetic materials, the total magnetization *M* is decomposed into its reversible (M_{rev}) and irreversible (M_{irr}) contribution as shown mathematically in equation (3). From a physical point of view, M_{rev} and M_{irr} are associated with the magnetic domain rotation and the wall displacements, respectively.

$$M = M_{rev} + M_{irr} \tag{3}$$

The anhysteretic magnetization M_{anh} can be described by the Langevin equation [21]:

*Corresponding author.
E-mail address: gael.sebald@insa-lyon.fr (Gael Sebald)

$$M_{anh} = M_s \left[\coth\left(\frac{H_e}{a}\right) - \frac{a}{H_e} \right] \tag{4}$$

or by using a hyperbolic function:

$$M_{anh} = M_s \tanh\left(\frac{H_e}{a}\right) \tag{5}$$

In both equations (4) and (5), M_{anh} is the anhysteretic magnetization, H_e is the effective field, M_s is the saturation magnetization, and a is the parameter describing the magnetic-field-dimension characteristic of the anhysteretic magnetization shape. According to the J-A theory, $a = k_B.T / \mu_0.m$, where k_B is Boltzmann's constant, T is the temperature, and m is the magnetic moment of a typical domain.

$$H_e = H + \alpha.M \tag{6}$$

Here, H, M, and α are the applied tangent excitation field, average sample magnetization, and mean field parameter related to the inter-domain coupling, respectively. The anhysteretic, irreversible, and reversible magnetization are related as follows:

$$M_{rev} = c(M_{an} - M_{irr}) \tag{7}$$

Where, c is a proportionality coefficient. This coefficient can be determined from the experimental results by calculating the ratio of the initial differential susceptibilities associated with the first and anhysteretic magnetization curves.

$$\frac{dM_{irr}}{dH_e} = \frac{M_{anh} - M_{irr}}{k\delta} \tag{8}$$

The coefficient k is the pinning parameter, which is linked to the amount of energy dissipated, and δ is a directional parameter, which ensures that energy is always lost through dissipation.

$$\begin{cases} \delta = +1 & if \quad dH/dt \geq 0 \\ \delta = -1 & if \quad dH/dt < 0 \end{cases} \tag{9}$$

Combining the aforementioned equations yields the main equation of the J-A model:

$$\frac{dM}{dH} = \frac{(1-c)\frac{dM_{irr}}{dHe} + c\frac{dM_{anh}}{dHe}}{1-\alpha(1-c)\frac{dM_{irr}}{dHe} - \alpha c\frac{dM_{anh}}{dHe}} \tag{10}$$

Variations in the magnetization M with respect to variations in H can be calculated from equation (10). However, for some applications (e.g., consideration of the dynamic effect), the magnetic induction B is known before H. References [19] and [20] detail the inverse version of the J-A model for ferromagnetic materials, where the model input is the magnetization B. The physical principles of the model are very similar and the main equation of this inverse model for ferromagnetic materials becomes:

$$\frac{dM}{dB} = \frac{(1-c)\frac{dM_{irr}}{dB_e} + \frac{c}{\mu_0}\frac{dM_{anh}}{dH_e}}{1+\mu_0(1-\alpha)(1-c)\frac{dM_{irr}}{dB_e} - c(1-\alpha)\frac{dM_{anh}}{dH_e}} \tag{11}$$

With

$$\frac{dM_{irr}}{dB_e} = \frac{M_{anh} - M_{irr}}{\mu_0 k\delta} \tag{12}$$

and

$$B_e = \mu_0.H_e \tag{13}$$

B_e is the effective magnetic flux density.

*Corresponding author.
E-mail address: gael.sebald@insa-lyon.fr (Gael Sebald)

5.2. A Jiles-Atherton-type approach for the simulation of the of MBN_{energy}(H) cycles

This simulation study is aimed at deriving a reliable parameter or a combination of parameters, which can be used to evaluate the microstructure of the material. As detailed in [15], MIP yields good correlations for the three modeling parameters, α, k, and c. For the B(H) measurements, α provides an interesting correlation [15]. The parameter/s applicable to measurements performed via the Magnetic Barkhausen Noise technique is/are determined. The simulation process must be run prior to the correlation step. For the MBN_{energy} hysteresis cycle, this process starts with the approximation of the experimental MBN_{energy} anhysteretic curve. For this curve, we have opted for a numerical estimation rather than experimental measurements. We proceed in this manner because the experimental procedure is tedious and the estimated anhysteretic curves of almost all the classical soft magnetic materials differ only slightly from the measured curves. Assuming that the major hysteresis cycle is perfectly symmetrical, the MBN_{energy} anhysteretic curve can be calculated from the increasing and decreasing parts of the cycle equation:

$$H_i^{anhyst}(B_i) = \frac{H_i^{inc}(B_i) + H_i^{dec}(B_i)}{2} \tag{14}$$

Here, H_i^{inc}, H_i^{dec} and H_i^{anhyst} represent the H values corresponding to the increasing part and decreasing part of the major hysteresis cycle, and the anhysteretic cycle, respectively. M_s and a, the Jiles-Atherton anhysteretic parameters are calculated by fitting the estimated anhysteretic curve to the simulated curve using Matlab™ curve fitting toolbox. An optimization code based on the minimization of an error function (eq. 15) is used to determine the optimal α, k, and c combination.

$$\begin{gathered} dH/dt > 0, \qquad H \in \left[H_{\min}, H_{\max}\right] \\ Error = \sum_{i=1}^{n} abs\left(\left|MBN_{energy}\right|_i^{\exp}(H_i) - \left|MBN_{energy}\right|_i^{sim}(H_i)\right) \end{gathered} \tag{15}$$

5.3. Modeling parameters derived from simulation of MBN_{energy} curves

A simulated and a measured MBN_{energy} hysteresis cycle for sample 1 are compared in Fig. 11. In Fig. 11(b), the modeling parameter (*k* in this case) is derived from the fitting of the simulated curve to the experimental curve. An analysis of the simulation parameters reveals that the most relevant correlation occurs for the coefficient *k* (Fig. 11(b)). This is verified by calculating the Pearson Correlation coefficient, as shown in Fig. 12. *k* is evaluated with different (mechanical, magnetic, and mathematical) parameters and a correlation is determined using the Pearson correlation coefficient (for *k* and *α*), as shown in Fig. 12. The value of the coefficient increases with increasing strength of the correlation (values close to 1/-1 indicate a strong (positive/negative) correlation).

*Corresponding author.
E-mail address: gael.sebald@insa-lyon.fr (Gael Sebald)

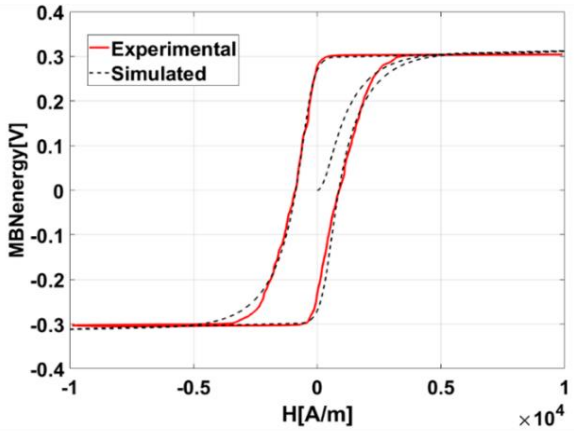

(a) Simulated and Experimental MBN_{energy} Curves for Sample 1

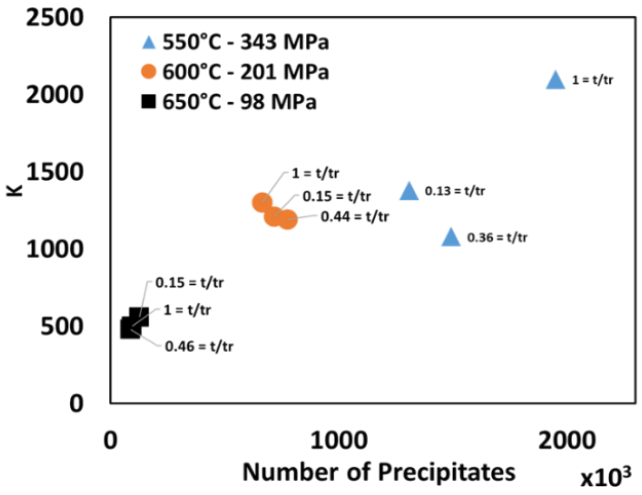

(b) Evolution of k parameter versus Precipitates

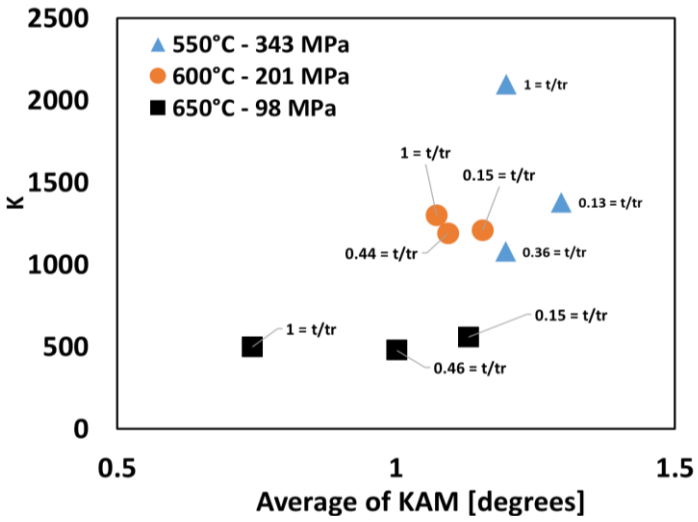

(c) Evolution of k parameter versus Average of KAM

Figure 11. Comparison of simulated and experimental curves for sample 1 MBN_{energy} cycle, dependence of the k coefficient on the number of precipitates, dependence of the k coefficient on KAM

*Corresponding author.
E-mail address: gael.sebald@insa-lyon.fr (Gael Sebald)

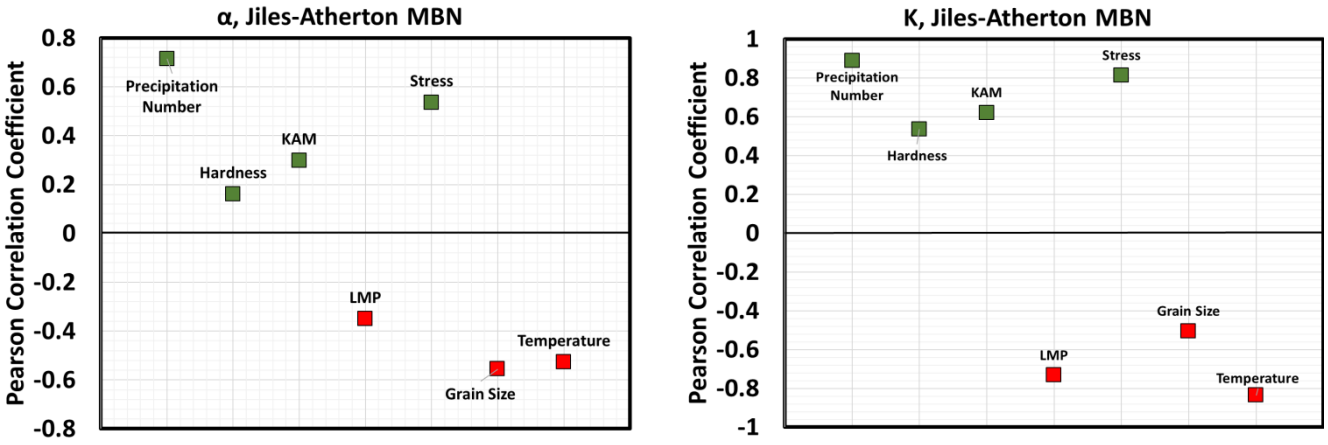

(a) Pearson correlation coefficient for α *(b) Pearson correlation coefficient for k*

Figure 12. Pearson coefficient for comparisons between simulation parameters (α, k) and microstructural parameters

The J-A parameters are all inter-related, i.e., each parameter changes with changes in the values of the other parameters. Hence, the most stable parameter (*k* in this case) with variations in other parameters (*α, c*), which corresponds to the coercivity of the materials in this case, is chosen. The 550°C sample contains more dislocations and precipitates (Microstructural Analysis, section 3) than the other samples and, hence, the *k* factor of this sample is higher (in general) than those of the other samples (see Fig. 11). A comparison of Fig. 9(a) and Fig. 11(b), which show the coercivity vs. the number of precipitates and *k* vs. the number of precipitates, respectively, reveals quite similar tendencies. However, some variations are expected since, *k* is also associated with the effect of the variations in other parameters (*α*, *c*). The variation in the *k* parameter vs. the creep life fraction t/t_r (see Fig. 13) confirms that the evolution trend of the 550°C samples is opposite to that of the 650°C samples. However, the rate of change is also an important factor. In the 550°C samples, the change rate of *k* with increasing rupture time is considerably higher (in the increasing direction) than the quite small change rate in the 650°C samples (in the decreasing direction). From the precipitation point of view, the high-temperature samples (650°C) exhibit only modest variations, but regarding dislocations, these samples exhibit larger variations when *k* vs. the average of KAM is considered (see Fig. 11(c)). The variation with respect to KAM observed for the magnetic and model parameters corresponding to the higher temperature samples is larger (also the case for MIP [15]) than that observed for the lower-temperature samples. Moreover, in the case of MBN, other parameters (e.g., α) are sensitive to only lower temperature samples and c is sensitive to only higher temperature samples. α represents the inter-domain coupling (Jiles-Atherton theory), which is higher for lower temperature samples since the precipitates are smaller than those in the higher temperature samples.

*Corresponding author.
E-mail address: gael.sebald@insa-lyon.fr (Gael Sebald)

Fig. 13 shows the evolution of the most reliable parameter (*k*) for the Magnetic Barkhausen noise in relation to the rupture level. Despite minor discrepancies, the overall evolution tendency of this parameter is quite similar to that of the coercivity factor derived from MBN_{energy} hysteresis cycles.

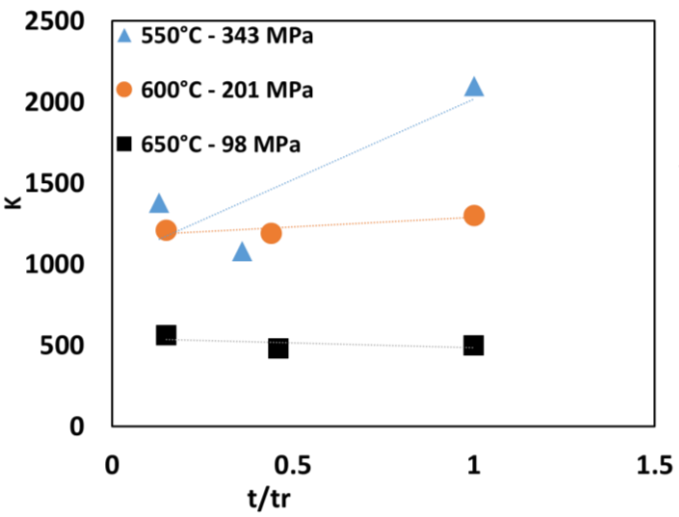

(a) Dependence of k on the rupture level characterizing samples treated at different temperatures

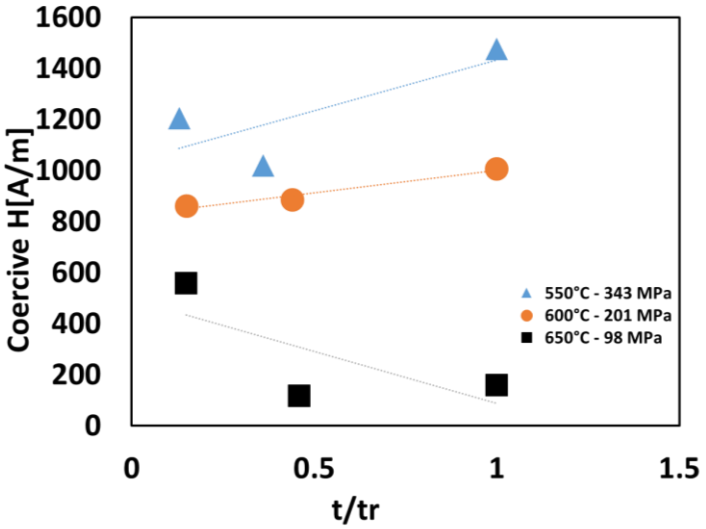

(b) Dependence of coercivity on the rupture level characterizing samples treated at different temperatures demonstrating similar evolution as k

Figure 13. Evolution of k and coercivity factor with respect to rupture level.

6. Conclusion

This work focuses on a micro-magnetic Magnetic Barkhausen Noise method for evaluating the microstructural state of 12 Cr-Mo-W-V steel. Such micro-magnetic analysis is of major interest as the microstructural state is deeply connected to flaw propagation in these structural steels and, if left unchecked, this propagation leads to severe problems. As a means of revealing the magnetic domain wall movements, the Barkhausen noise measurement is a micro-magnetic non-destructive testing method of significant potential and interest. In this study, rather than following the classical approach, which consists of working directly from the raw signal, $MBN_{energy}(H)$ hysteresis cycles have been reconstructed and simulated. Working with these cycles limits the reproducibility and the sensitivity issues (such as providing a magnetic signature). The amplitude of each MBN_{energy} curve decreases (in general) with increasing creep level. Furthermore, based on the observed hysteresis, these MBN_{energy} curves can be easily simulated using the classical hysteresis models, such as the Jiles-Atherton model, which has been used in this study. Experimental tests and simulations are followed by a detailed analysis aimed at determining the correlations between the magnetic parameters (coercive field, permeability factor), J-A simulation parameters, and the microstructural properties. For example, a correlation factor of ~0.9 is obtained when the *k* parameter is considered with respect to the number of precipitates and an α of 0.8.

*Corresponding author.
E-mail address: gael.sebald@insa-lyon.fr (Gael Sebald)

Acknowledgment

This work was performed in the framework of the Japan - France International Laboratory (LIA) ELyTGlobal. The authors gratefully acknowledge the French Region Auvergne-Rhône-Alpes, the French project IDEXLYON of the Université de Lyon in the framework of the "Investissements d'Avenir" program (ANR-16-IDEX-0005), and the Institute of Fluid Science (Tohoku University) through the General Collaborative Program projects # J17I065, #J18I055, and the JSPS KAKENHI Grant, #18H01448.

References

[1] J. Gauthier, T.W. Krause, D.L. Atherton, "Measurement of residual stress in steel using the magnetic Barkhausen noise technique", NDT&E Int. vol. 31, iss. 1, pp. 23-31, 1998.

[2] H.I. Yelbay, I. Cam, C.H. Gür, "Non-destructive determination of residual stress state in steel weldments by magnetic Barkhausen noise technique", NDT&E Int. vol. 43, iss. 1, pp. 29-33, 2010.

[3] G. Dobmann, I. Altepeter, B. Wolter, R. Kern, "Industrial applications of 3MA – Micromagnetic Multiparameter Microstructure and Stress Analysis", Electromagnetic Nondestructive Evaluation (IX), IOS Press, 2008.

[4] I. Altpeter, G. Dobmann, M. Kröning, M. Raboug, S. Szielasko, "Micro-magnetic evaluation of micro residual stresses of the IInd and III order", NDT&E Int., vol. 42, pp. 283-290, 2009.

[5] D.M. Stewart, K.J. Stevens, A.B. Kaiser, "Magnetic Barkhausen noise analysis of stress in steel", Cur. App. Phys., pp. 308-311, 2004.

[6] X. Kleber, A. Vincent, "On the role of residual internal stresses and dislocation on Barkhausen in plastically deformed steel", NDT&E Int., vol. 37, iss. 6, pp. 439-445, 2004.

[7] B. Gupta, T. Uchimoto, B. Ducharne, G. Sebald, T. Miyazaki, T. Takagi, "Magnetic incremental permeability non-destructive evaluation of 12 Cr-Mo-W-V Steel creep test samples with varied ageing levels and termal treatments", NDT&E Int., vol. 104, pp. 42-50, 2018.

[8] G. Sposito, "A review of non-destructive techniques for the detection of creep damage in power plant steels", NDT&E Int., 2010.

[9] Garofalo F. Fundamentals of creep and creep-rupture in metals. New York: Macmillan; 1965.

[10] B. Ducharne, B. Gupta, Y. Hebrard, J. B. Coudert, "Phenomenological model of Barkhausen noise under mechanical and magnetic excitations", IEEE Trans. Mag., vol. 99, pp. 1-6, 2018.

[11] B. Ducharne, MQ. Le, G. Sebald, PJ. Cottinet, D. Guyomar, Y. Hebrard, "Characterization and modeling of magnetic domain wall dynamics using reconstituted hysteresis loops from Barkhausen noise", J. Magn. Magn. Mater., pp. 231-238, 2017.

[12] Y. Mutoh, "Improving Fretting Fatigue Strength at Elevated Temperatures by Shot Peening in Steam Turbine Steel, Standardization of Fretting Fatigue Test Methods and Equipment", ASTM STP 1159, M. Helmi Attia and R.B. Waterhouse, Eds., American Society for Testing and Materials, Philadelphia, 1992, pp.119-209.

[13] F. R. Larson, J. Miller, Transactions ASME, Vol. 74, p. 765–771, 1952.

*Corresponding author.
E-mail address: gael.sebald@insa-lyon.fr (Gael Sebald)

[14] C. Moussa, “About quantitative EBSD analysis of deformation and recovery substructures in pure Tantalum bout quantitative EBSD analysis of deformation and recovery substructures in pure Tantalum”, 36th Risø International Symposium on Materials Science. 2015.

[15] B. Gupta, B. Ducharne, G. Sebald, T. Uchimoto, T. Miyazki, T. Takagi, “Physical interpretation of the microstructure for aged 12 Cr-Mo-V-W steel creep test samples based on simulation of magnetic incremental permeability”, J. Magn. Magn. Mater., vol. 486, 2019.

[16] D. C. Jiles and D. L. Atherton, “Theory of ferromagnetic hysteresis”, J. Magn. Magn. Mater., vol. 61, nos. 1–2, pp. 48–60, 1986.

[17] D. C. Jiles, “A self-consistent generalized model for the calculation of minor loop excursions in the theory of hysteresis”, IEEE Trans. Mag., vol. 28, no. 5, pp. 2602–2604, 1992.

[18] B. Zhang, B. Gupta, B. Ducharne, G. Sebald, T. Uchimoto, “Dynamic magnetic scalar hysteresis lump model based on Jiles-Atherton quasi-static hysteresis model extended with dynamic fractional derivative contribution”, IEEE Trans. Mag., vol. 54, iss. 11, 2018.

[19] J. V. Leite, N. Sadowski, P. Kuo-Peng, N. J. Batistela, and J. P. A. Bastos, “The inverse Jiles-Atherton model parameters identification”, IEEE Trans. Magn., vol. 39, no. 3, pp. 1397–1400, May 2003.

[20] J. V. Leite, N. Sadowski, P. Kuo-Peng, N. J. Batistela, J. P. A. Bastos, and A. A. de Espindola, “Inverse Jiles–Atherton vector hysteresis model”, IEEE Trans. Mag., vol. 40, no. 4, pp. 1769–1775, Jul. 2004.

[21] R. Zwanzig, “Nonlinear generalized Langevin equations”, J. of Stat. Phys, vol. 9, Iss. 3, pp. 2215-220, 1973.

*Corresponding author.
E-mail address: gael.sebald@insa-lyon.fr (Gael Sebald)